Available online at www.sciencedirect.com
SCIENCE DIRECT®
Polymer 44 (2003) 3579–3591
polymer
www.elsevier.com/locate/polymer

Localisation phenomena in glassy polymers: influence of thermal and mechanical history

H.G.H. van Melick, L.E. Govaert*, H.E.H. Meijer

Dutch Polymer Institute (DPI), Section Materials Technology (MaTe), Eindhoven University of Technology, P.O. Box 513, NL-5600MB Eindhoven, The Netherlands

Received 1 July 2002; received in revised form 23 January 2003; accepted 24 January 2003

Abstract

The macroscopic deformation behaviour of amorphous polymers is dominated by localisation phenomena like necking and crazing. Finite element simulations show that the details of the intrinsic post-yield behaviour, strain softening and strain hardening, determine the severity of strain localisations. In order to perform these numerical simulations an accurate constitutive model is required. The compressible Leonov model is, for this purpose, extended to include temperature effects. Experimentally it is demonstrated that by a small increase in strain softening (by annealing of polycarbonate) or substantial decrease (by mechanical rejuvenation of polystyrene), transitions from ductile to brittle and, respectively, brittle to ductile can be realised. An analytical stability analysis is performed that predicts stable or unstable neck growth dependent on the ratio between yield stress and hardening modulus. The extensive simulations and experimental results lead to the conclusion that in order to macroscopically delocalise strain, and thus improve toughness, one has to reduce strain softening or enhance strain hardening, either by improving the intrinsic behaviour of polymers, or by creating an optimised micro-structure.

Keywords: Glassy polymers; Strain localisation; Thermo-mechanical history

1. Introduction

The macroscopic deformation behaviour of amorphous polymers is generally dominated by localisation phenomena like shear-band formation, necking and crazing. Which mechanism prevails during deformation is determined by the post-yield behaviour, specifically the balance between strain softening and strain hardening. Although all glassy polymers show a similar intrinsic post-yield behaviour, their macroscopic behaviour is quite different. Polystyrene is, for instance, an extremely brittle material. In tension, crack-like defects appear already in the apparent elastic region. These lens-shaped defects, so-called *crazes*, are no actual cracks but the faces are still bridged with highly stretched fibrillar material [1,2], which provide them some load-bearing capacity. Ultimately, one of the crazes breaks up and looses its load-bearing capacity, resulting in macroscopic failure. Polycarbonate on the other hand, is a ductile material. In tension, upon yielding, a stable neck is formed that proceeds along the tensile bar and fails at elongations exceeding a draw ratio of approximately 2.

The marked difference in macroscopic behaviour between polystyrene and polycarbonate can be rationalised in terms of subtle differences in strain softening and strain hardening [3]. In polystyrene localisation of strain is severe due to pronounced strain softening and, since its strain hardening is weak, these strain localisations evolve to extremes, leading to crazing and brittle fracture. The moderate strain softening of polycarbonate does induce strain localisations that are, however, easily stabilised by its strong strain hardening contribution.

Many examples are known considering the influence of strain hardening on the macroscopic deformation behaviour. It is now well established that strain hardening is a stress contribution of the entangled polymer network [4–6], the strongest arguments being that it can be enhanced by increasing the network density. For polystyrene this can be achieved by cross-linking [6,7] or by blending with polyphenylene oxide (PPO) [6,8]. The increase in strain hardening eventually leads to macroscopically ductile deformation behaviour in polystyrene, for instance, Henkee

* Corresponding author. Tel. +31-40-2472838; fax: +31-40-2447355.
E-mail address: l.e.govaert@tue.nl (L.E. Govaert).

0032-3861/03/$ - see front matter © 2003 Elsevier Science Ltd. All rights reserved.
doi:10.1016/S0032-3861(03)00089-2

and Kramer [7] reported that cross-linking of polystyrene induced a transition from crazing to shear yielding in a tensile test. Similar results were reported for blends of polystyrene and polyphenylene oxide (PPO) with high fractions of PPO [9–13].

Although the exact physical origin of strain softening is not really clear, it is known to be strongly related to physical ageing [14,15]. Physical ageing is often explained by the free volume theory [15], despite the fact that there is evidence that questions this relation. During mechanical treatments or tests, in which the material is rejuvenated and strain softening is reduced, the macroscopic density increased and thus free volume must have decreased [16–18]. Furthermore, it is known that strain softening depends on the thermal and mechanical history and the testing conditions. Quenched samples exhibit less strain softening than slowly cooled specimens [17,19,20], strain softening can be drastically reduced, or even eliminated, by mechanical pre-conditioning or pre-deformation [5,17, 21–25] and, similar to the yield stress, strain softening is sensitive to temperature, strain rate and pressure [26–29].

In this paper the influence of post-yield behaviour on localisation of strain during deformation is investigated by numerical and experimental methods. Finite element simulations, employing the compressible Leonov model, are performed to show the consequences of differences in intrinsic behaviour on macroscopic deformation behaviour of polystyrene and polycarbonate. Only localisation of strain is considered and failure mechanisms, which occur in this process [30–32], are not incorporated. The influence of thermal and mechanical treatments on softening and the consequences for macroscopic deformation behaviour are investigated. Finally, finite element simulations are used to illustrate the influence of temperature and a supporting rubber layer on the macroscopic deformation behaviour of polystyrene in tension.

2. Materials and methods

2.1. Materials

The materials used were a commercial grade of polystyrene, N5000 (supplied by Shell) and two commercial grades of polycarbonate, Lexan 101^{R} (supplied by General Electric Plastics) and Makrolon CD2000 (supplied by Bayer Co.). For the uniaxial compression tests, cylindrical samples ($\varnothing$ 6 mm × 6 mm) were machined from thick plates (160 × 160 × 9 mm^3), which were compression moulded from granular material at a temperature 90 °C above their T_g. First the material was heated for 15 min in the mould and compressed during 5 min in 5 steps of increasing force, up to a maximum force of 300 kN. In between the steps, the force was released to allow for degassing. Afterwards, the mould was placed in a cold press and cooled to room temperature at a moderate force (100 kN). The specimens for the uniaxial tensile tests were made via injection moulding, according to ISO 527. Prior to processing, all materials were dried in a oven at 70 °C for 3 days.

2.2. Mechanical tests

Uniaxial compression and tensile tests were performed on a servo-hydraulic MTS Elastomer Testing System 810. In compression tests, specimens were loaded between two parallel, steel compression plates. Friction between sample and plates was reduced by an empirically optimised method: onto the sample a thin film of PTFE tape (3M 5480, PTFE skived film tape) was applied and the surface between steel and tape was lubricated by a soap–water mixture. During compression tests, no bulging or buckling of the sample was observed, indicating that the friction was sufficiently reduced. The compression tests were performed, in strain control, at constant logarithmic strain rates ranging from 10^{-4} to 10^{-2} s^{-1} whereas uniaxial tensile tests were performed at a constant linear strain rate of 10^{-3} s^{-1}. A temperature chamber was used to allow accurate control of the temperature (±0.5 °C). Approximately 15 min prior to testing the samples were mounted in the setup to ensure thermal equilibrium at the desired temperature.

2.3. Thermo-mechanical treatments

Two thermal treatments were used: quenching and annealing. Quenching was performed by heating of the samples in an oven at 15 °C above their glass transition temperature for half an hour and, subsequently, rapidly cooling in ice–water. The annealing was done by a heating period of three days at 20 °C below the glass transition temperature, followed by slow cooling (1 day) to room temperature. The mechanical treatment of polystyrene (rolling) is extensively described in Govaert et al. [25].

2.4. Intrinsic deformation behaviour

2.4.1. Uniaxial compression tests

Since localisation phenomena like necking and crazing are suppressed in uniaxial compression tests, these tests are used here to determine the intrinsic deformation behaviour of polystyrene and polycarbonate. Fig. 1 shows the true-stress/true-strain curves at a temperature of 20 °C and a logarithmic strain rate of 10^{-3} s^{-1} (circles). The differences in intrinsic behaviour between polystyrene and polycarbonate are unambiguously shown. Besides a slight difference in elastic modulus and yield stress, the main difference is found in the amount of strain softening, or yield drop, and in the value of the strain hardening modulus.

Polystyrene exhibits a yield drop of approximately 30 MPa, whereas for polycarbonate this drop is only 19 MPa under identical testing conditions. The strain hardening modulus, defined as the slope of the stress–strain curve (true stress versus $\lambda^2 - \lambda^{-1}$ at large strains, is

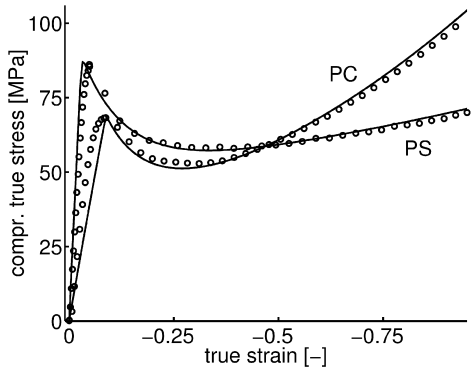

Fig. 1. True-stress/true-strain curves for PS and PC in compression: experimental data (circles) and numerical simulations (solid lines), using the compressible Leonov model with the parameters given in Table 1.

more than twice as large for polycarbonate as for polystyrene, 29 MPa versus 11 MPa.

2.4.2. Numerical modelling

The numerical model used here will be referred to as the 'generalised compressible Leonov model' [24,33], after the original paper of Tervoort et al. [33]. In this model, a distinction is made between the contribution of secondary interactions between polymer chains, which determine the (visco-) elastic properties at small deformations and the yield behaviour, and the entangled polymer network that governs the large strain behaviour.

The total Cauchy stress $\boldsymbol{\sigma}$ is decomposed in a driving stress ($\mathbf{s}$) and a hardening stress ($\mathbf{r}$) according to:

$$\boldsymbol{\sigma} = \mathbf{s} + \mathbf{r} \tag{1}$$

The driving stress is subsequently decomposed into a deviatoric part $\mathbf{s}^{\mathrm{d}}$ hydrostatic part ($\mathbf{s}^{\mathrm{h}}$) :

$$\mathbf{s}^{\mathrm{d}} = G\tilde{\mathbf{B}}_{\mathrm{e}}^{\mathrm{d}}, \qquad \mathbf{s}^{\mathrm{h}} = \kappa(J-1)\mathbf{I} \tag{2}$$

where G is the shear modulus, $\tilde{\mathbf{B}}_{\mathrm{e}}^{\mathrm{d}}$ the deviatoric part of the isochoric elastic left Cauchy–Green deformation tensor, κ the bulk modulus, J the volume change factor and $\mathbf{I}$ the unity tensor. The superscripts d and h denote the *deviatoric* and the *hydrostatic* part, respectively, the subscripts e, p, and eq indicate that an *elastic*, *plastic*, and *equivalent* quantity is used. The relative volume change and the isochoric elastic left Cauchy–Green deformation tensor $\tilde{\mathbf{B}}_{\mathrm{e}}$, are given by the evolution equations:

$$\dot{J} = J\cdot\mathrm{tr}(\mathbf{D}) \tag{3}$$

$$\overset{\circ}{\tilde{\mathbf{B}}}_{\mathrm{e}} = (\mathbf{D}^{\mathrm{d}} - \mathbf{D}_{\mathrm{p}})\cdot\tilde{\mathbf{B}}_{\mathrm{e}} + \tilde{\mathbf{B}}_{\mathrm{e}}\cdot(\mathbf{D}^{\mathrm{d}} - \mathbf{D}_{\mathrm{p}}) \tag{4}$$

where $\overset{\circ}{\tilde{\mathbf{B}}}_{\mathrm{e}}$ is the Jaumann rate of $\tilde{\mathbf{B}}_{\mathrm{e}}$, $\mathbf{D}^{\mathrm{d}}$ the deviatoric part of the rate of deformation tensor and $\mathbf{D}_{\mathrm{p}}$ the plastic part of the rate of deformation tensor.

The hardening behaviour is described by a neo-Hookean relation for the hardening stress $\mathbf{r}$:

$$\mathbf{r} = G_{\mathrm{R}}\tilde{\mathbf{B}}^{\mathrm{d}} \tag{5}$$

where G_{R} is the strain hardening modulus. As proposed by Tervoort et al. [33] a Newtonian flow rule with a stress dependent Eyring viscosity is used to relate the plastic deformation rate tensor, $\mathbf{D}_{\mathrm{p}}$, to the deviatoric driving stress tensor, $\mathbf{s}^{\mathrm{d}}$:

$$\mathbf{D}_{\mathrm{p}} = \frac{\mathbf{s}^{\mathrm{d}}}{2\eta(\tau_{\mathrm{eq}}, D, p)} \tag{6}$$

The viscosity, η, is strongly dependent on the equivalent stress, τ_{eq}, and was originally described by an Eyring relationship [34]. Govaert et al. [24] extended the model by incorporating pressure dependence (μ) and intrinsic strain softening (D) in the viscosity function:

$$\eta(\tau_{\mathrm{eq}}, D, p) = A(D,p)\tau_0 \frac{\dfrac{\tau_{\mathrm{eq}}}{\tau_0}}{\sinh\left(\dfrac{\tau_{\mathrm{eq}}}{\tau_0}\right)} \tag{7}$$

where the equivalent stress, τ_{eq}, is defined as:

$$\tau_{\mathrm{eq}} = \sqrt{\frac{1}{2}\mathrm{tr}(\mathbf{s}^{\mathrm{d}}\cdot\mathbf{s}^{\mathrm{d}})} \tag{8}$$

and

$$A = A_0 \exp\left(\frac{\Delta H}{RT}\right)\exp\left(\frac{\mu p}{\tau_0} - D\right) \tag{9}$$

$$\tau_0 = \frac{RT}{V} \tag{10}$$

$$p = -\frac{1}{3}\mathrm{tr}(\boldsymbol{\sigma}) = -\frac{1}{3}\mathrm{tr}(\mathbf{s}) \tag{11}$$

where A_0 is a constant pre-exponential factor, R the gas constant, and T is the absolute temperature. In the evolution of the softening, originally proposed by Hasan et al. [35], the softening parameter D is initially set to zero. In time, this parameter evolves to the softening limit D_∞ according to:

$$\dot{D} = \left(1 - \frac{D}{D_\infty}\right)\dot{\gamma}_{\mathrm{p}} \tag{12}$$

where the equivalent plastic strain rate, $\dot{\gamma}_{\mathrm{p}}$, equals:

$$\dot{\gamma}_{\mathrm{p}} = \sqrt{2\mathrm{tr}(\mathbf{D}_{\mathrm{p}}\cdot\mathbf{D}_{\mathrm{p}})} \tag{13}$$

From Eq. (6a) a condensation in equivalent quantities can be performed using Eqs. (8) and (13), under the assumption that during yielding the equivalent strain rate equals the equivalent plastic strain rate:

$$\dot{\gamma}_{\mathrm{eq}} = \frac{\tau_{\mathrm{eq}}}{\eta(\tau_{\mathrm{eq}}, D, p)} \tag{14}$$

Combining this equation with Eq. (7) yields the well-known Eyring expression for the equivalent strain rate as function of the equivalent stress [34]:

$$\dot{\gamma}_{\mathrm{eq}} = \frac{1}{A}\sinh\left(\frac{\tau_{\mathrm{eq}}}{\tau_0}\right) \tag{15}$$

If the argument of the hyperbolic sine function is large, it

can be replaced by an exponential function. Some rearrangement of Eqs. (9) and (15) (at yield point $D = 0$), results in an equation for the equivalent stress, expressed in the equivalent strain rate:

$$\tau_{eq} = \tau_0 \left[\ln(2A_0 \dot{\gamma}_{eq}) + \frac{\Delta H}{RT} + \frac{\mu p}{\tau_0} \right] \tag{16}$$

This expression can be used directly to fit the parameters on the experimental data, the macroscopic yield stresses (σ_y) and the logarithmic strain rates ($\dot{\varepsilon}$). Using Eqs. (8) and (13) in a uniaxial compression test, at the yield point, equivalent quantities can be expressed as function of stress and strain rate:

$$\tau_{eq} = \frac{1}{\sqrt{3}} \sigma_y, \qquad \dot{\gamma}_{eq} = \sqrt{3}\dot{\varepsilon} \tag{17}$$

In Fig. 2a, the experimentally obtained equivalent yield stresses, τ_{eq} (markers), as function of temperature and equivalent strain rate, $\dot{\gamma}_{eq}$, are presented. From the slope of these curves the characteristic stress, τ_0, and thus the activation volume V (see Eq. (10)) can be derived. From the offset of the curves at various temperatures the time constant, A_0, and the activation energy, ΔH, are determined. Since at a sufficiently high pressure ductile deformation behaviour is observed even in polystyrene, the pressure coefficient, μ, was determined up-front in a uniaxial tensile test under superimposed pressure at the IRC in Leeds and

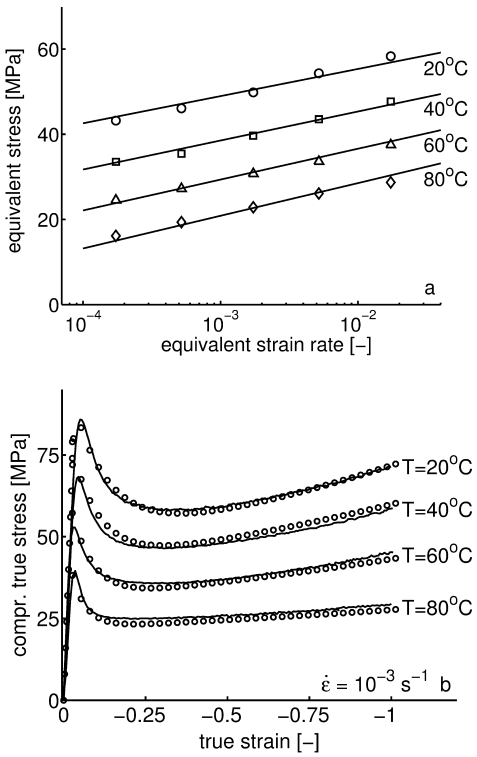

Fig. 2. Equivalent yield stresses of PS as function of equivalent strain rate and temperature (a) and the compressive behaviour of PS at various temperatures (b), markers represent the experiments, solid lines the simulations using the parameters given in Table 1.

proved to be equal to 0.14. The solid lines in Fig. 2a are fits with the parameters for PS N5000 given in table 1. For the elastic parameters E and ν literature values are taken [36].

The strain hardening modulus is determined from the slope of the stress–strain curve at large strains. The last two parameters, the softening limit, D_∞, and the softening slope, h, are obtained by a visual fit on the true stress–strain curve of a uniaxial compression test at 20 °C and 10^{-3} s^{-1}, see Fig. 2b. The parameters derived under these testing conditions are the reference values and will be referred to with the subscript 0. The material parameters used in the simulations are given in Table 1.

Since the temperature not only influences the yield stress, but also has a significant influence on modulus, softening limit and strain hardening, a temperature dependence of these properties for polystyrene is incorporated in the simulations. The temperature dependence of the modulus is derived from dynamical mechanical thermal analysis [6] and reads:

$$E(T) = E_0(-0.0264T + 1.79) \tag{18}$$

Although for visco-elastic materials a more complex relation would be appropriate, for the isothermal simulations this simple relation is adequate. From this temperature dependent modulus and the Poisson ratio the bulk modulus, κ, and shear modulus, G are derived which are used a input in the numerical model. The temperature dependence of the strain hardening modulus and the softening limit are derived from uniaxial compression tests at various temperatures, see Fig. 2b, and yields:

$$D_\infty(T) = D_{\infty,0}(-0.012T + 4.516)$$

$$G_R(T) = G_{R,0}(-0.0133T + 4.91) \tag{19}$$

In these empirical relations T (K) is the absolute temperature. Since the value of the strain softening parameter D evolves in time according to Eq. (12), the assumed temperature dependence can only be used in stationary temperature fields. The slight rate dependence of the strain softening [31] is not incorporated in the numerical model.

Apart from the difference in tensile strength and a slight difference in strain hardening modulus [38], the difference

Table 1
Material parameters of PS N5000 and/Lexan 101^R/Makrolon CD2000

	PS N5000	Lexan 101^R/Makrolon CD2000
E (Mpa)	3300	2400
ν [–]	0.37	0.4
V (m^3 mol^{-1})	9.52×10^{-4}	3.4×10^{-3}
ΔH (J mol^{-1})	1.70×10^5	2.9×10^5
A_0 (s)	1.11×10^{-20}	3.6×10^{-25}
G_R (Mpa)	11	29
D_∞ (–)	9	26
h (–)	60	200
μ (–)	0.14	0.07

in molecular weight (distribution) for the polycarbonate grades has no influence on the intrinsic properties, and hence the same parameter set is used for Lexan 101^{R} and Makrolon CD2000, adopted from Ref. [24].

The solid lines in Figs. 1 and 2b represent the numerical simulations using the parameter sets from Table 1 and demonstrate the ability of the compressible Leonov to give a quantitative description of the intrinsic deformation behaviour of glassy polymers.

2.4.3. FEM model

The geometry used in the finite element simulations is an axisymmetric model of a tensile bar with a small imperfection, situated at the surface in the middle of the tensile bar. The cylindrical tensile bar has a dimensionless parallel length of 1 and a radius of 0.2. The circular imperfection has a radius of 0.02 and a maximum depth of 0.003 (1.5% of the radius of the bar). Govaert et al. [24] showed that the size and shape of the imperfection are only of minor influence on the deformation of the tensile bar. Only the draw ratio during stable neck growth is slightly influenced. The finite element model consists of 537 8-noded second-order elements, shown in Fig. 3. During the tensile test the bar is deformed at a constant linear strain rate of $10^{-3}\,s^{-1}$. For the simulation in which a rubber layer is incorporated, a thin layer (10% of the radius of the bar) of elements is glued on the surface to the tensile bar. For the rubber a neo-Hookean model is chosen with a shear modulus of 150 MPa.

3. Results

3.1. Deformation and localisation processes in polycarbonate

3.1.1. Results of finite element simulations

Fig. 4 shows a numerical simulation of a tensile test on polycarbonate. During the initial elastic stage, stresses rise throughout the specimen and, until the yield point is reached, the stress is approximately equal in all marked positions. Yield and subsequent plastic deformation occurs first underneath the imperfection (bullet) and, immediately after yielding, the material deforms, localising the strain in this zone, accompanied by a local drop in stress because of strain softening. Both events cause the stress to drop in the elastically deformed regions and the other three markers descend along the elastic curve, see Fig. 4a.

With ongoing deformation, the material in the deformed region experiences strain hardening. As a result, the force required to deform this material exceeds the force required to induce yielding in the adjacent material (shoulder). Fig. 4b shows the stage in which the material in the neck (bullet) is stabilised and the shoulder (triangle) of the neck reaches the yield point. Next yielding occurs in the shoulder, while the material already present in the neck is not strained further. This continuing process of yielding, localisation and stabilisation results in formation of a stable neck that proceeds along the tensile bar (see Fig. 4c) until the neck reaches the tabs of the tensile bar (diamond). Then again the stress is quite homogeneously distributed throughout the tensile bar, which can be witnessed from the fact that all markers are approximately at the same position in the intrinsic stress–strain curve, see Fig. 4d. With ongoing deformation, cold-drawing in the neck proceeds until the tensile strength in the neck is exceeded.

The process of stabilisation of the neck can be demonstrated by the evolving stress and draw ratio in the neck during deformation. In Fig. 5, the engineering stress versus nominal draw ratio is plotted (solid line), which represents the macroscopic response in a tensile test. Stress rises until the yield stress in reached, followed by a sudden drop as the neck is formed. Throughout the process of necking, the engineering stress remains at a constant level. The dashed line in the graph represents the local draw ratio in the neck (underneath the imperfection), as function of the nominal draw ratio. Immediately after yielding, the draw ratio increases rapidly and levels off to a merely constant value, indicating that the deformation is stabilised in the neck. The exact value at which the neck is stabilised is of course dependent on the value of the yield stress, the strain softening, and strain hardening. Once the neck reaches the tabs of the tensile bar (Fig. 4d), stress and draw ratio increase again until failure occurs.

3.1.2. The influence of thermal history

The intrinsic behaviour of glassy polymers is known to be dependent on the thermal history [17,19] and Fig. 6 shows that annealing induces a slight increase in yield stress of, in this case, polycarbonate (Lexan 101^{R}). The change in strain softening (or yield drop) equals the increase in yield

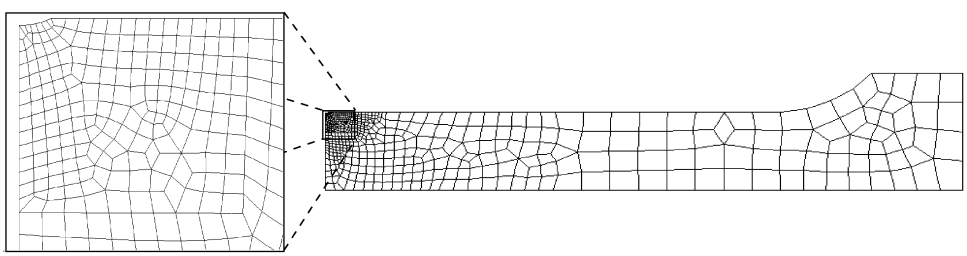

Fig. 3. Finite element mesh of the tensile bar with imperfection (zoomed area).

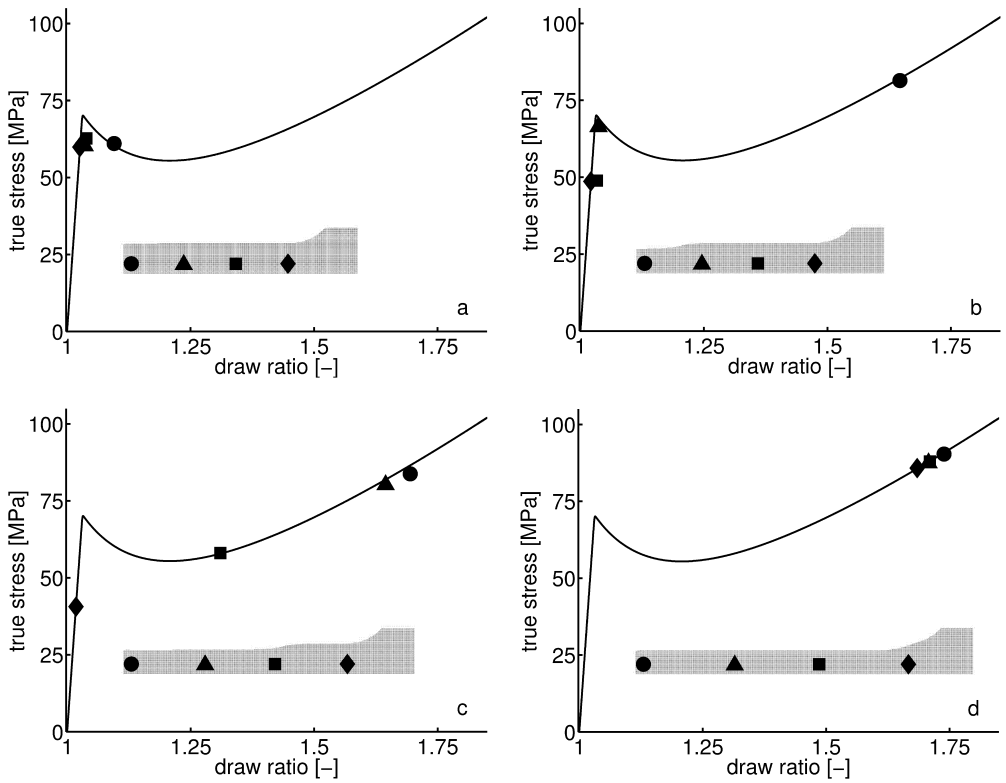

Fig. 4. Numerical simulation of a tensile test on PC: stable neck growth.

stress since the large strain behaviour (strain hardening), remains unaffected by annealing.

The subtle changes in strain softening can have major consequences for the macroscopic deformation behaviour. Fig. 7 shows the stress–strain curves of uniaxial tensile tests on Makrolon CD2000, before and after thermal treatment. For the injection moulded tensile bar, a neck appears shortly after yielding (see Figs. 7a and 8a) and the process continues as described before.

In the annealed material, brittle fracture is observed in the apparent elastic region, well below the macroscopic yield stress (see Figs. 7b and 8b). The enhanced intrinsic strain softening after annealing (see Fig. 6) induces a more severe localisation of strain during deformation, which, due to the limited tensile strength of this low molecular weight grade, cannot be stabilised.

That this brittle fracture is indeed caused by changes in intrinsic properties and not by degradation can be witnessed from the fact that the phenomenon is reversible. By bringing the annealed material again above its glass transition temperature and subsequent rapid cooling, stable neck growth is observed again in a tensile test (see Fig. 7c), similar to the behaviour of the injection moulded material prior to the treatments.

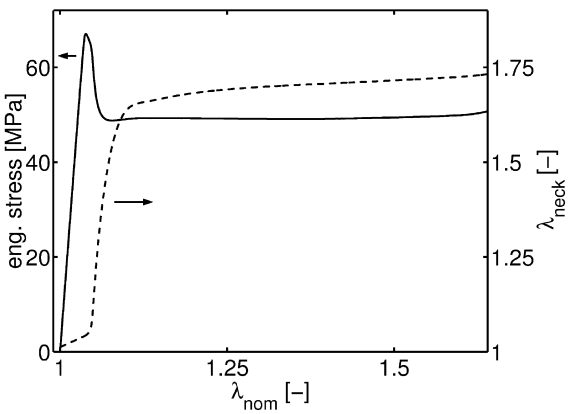

Fig. 5. Numerical tensile test on PC: engineering stress (solid) and draw ratio in the neck (dashed) versus the nominal draw ratio.

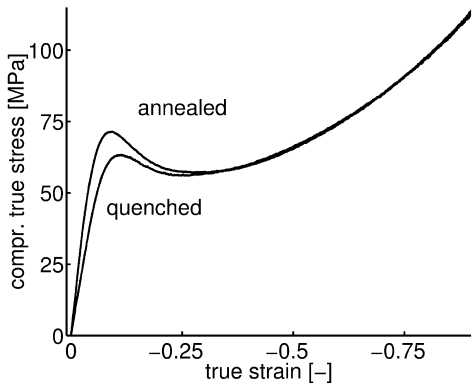

Fig. 6. Compression experiments demonstrating the influence of aging on the intrinsic behaviour of PC: an increase in yield stress and strain softening.

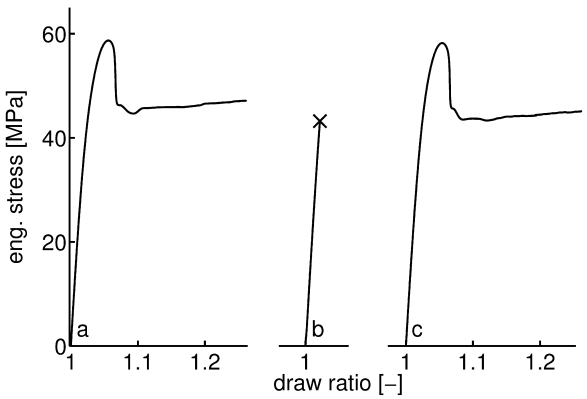

Fig. 7. Effect of thermal treatments on the macroscopic deformation: necking in injection moulded PC (a), embrittlement after annealing (b), and renewed necking after heating above T_g and subsequent rapid cooling (c).

3.1.3. The influence of mechanical history

Mechanical rejuvenation, also referred to as mechanical pre-conditioning or pre-deformation, has proven to be an effective method for the reduction, or even elimination, of strain softening. Bauwens [23] showed that by alternating bending prior to a tensile test, homogeneous deformation behaviour was achieved for PVC samples. Similar results were reported by Govaert et al. [24] and Tervoort and Govaert [5] who pre-conditioned cylindrical tensile bars of polycarbonate by torquing and studied macroscopic deformation behaviour before and after rejuvenation in tension. Uniaxial compression tests showed that the significant amount of strain softening (see Fig. 1) was eliminated while the large strain behaviour (strain hardening) remained unchanged. The elimination of strain softening prevented localisation of strain and neck-formation and hence the pre-conditioned samples exhibited uniform deformation behaviour. Figs. 8c and 12 show the homogeneous deformation of a rolled (thickness reduction of 15%) polycarbonate bar and illustrates this effect. It must be noted that strain softening restores in time; the yield stress and yield drop increase again, on a time scale of months, resulting in renewed neck formation in a uniaxial tensile test [37].

3.1.4. Results of a neck-stability analysis

The stability of macroscopic deformation in tension can be predicted if the intrinsic deformation behaviour, i.e. the yield stress, rejuvenated yield stress, and strain-hardening modulus are known up-front.

The approach of Haward [39] will be followed, who considered a material with no strain softening (yield stress equal to the rejuvenated yield stress $\sigma_{y,r}$, see Fig. 12a) and neo-Hookean strain hardening (with modulus G_R). Under the influence of ageing, the yield stress is assumed to increase according to: $\sigma_y = \kappa_y \sigma_{y,r}$, where κ_y is an arbitrary multiplier (larger than 1) that can be determined experimentally. This simple approach is not quite as accurate as the equations in the numerical model, but enables a straightforward neck-stability analysis.

A stable neck is formed if the load transferred by the neck equals the load required to induce yielding in the undeformed zone. Neglecting the small strain in the elastically deformed zones (i.e. $\lambda = 1$), the expression for equilibrium is given by:

$$\kappa_y \sigma_{y,r} A_i = \left[\sigma_{y,r} + G_R \left(\lambda_n^2 - \frac{1}{\lambda_n} \right) \right] \frac{A_i}{\lambda_n} \tag{20}$$

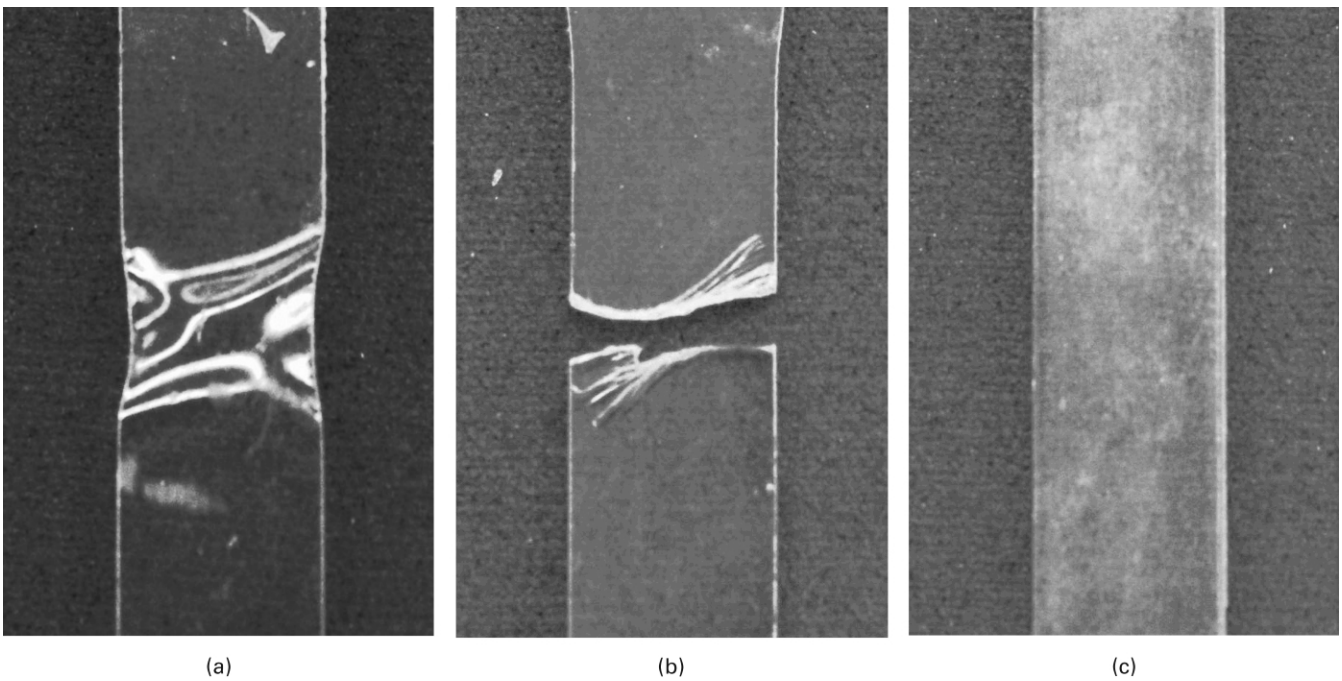

Fig. 8. Influence of thermo-mechanical history on macroscopic deformation of Makrolon CD2000, from necking in the injection moulded material (a), to brittle fracture after annealing (b) and homogeneous deformation after rolling (c).

where A_i is the initial cross-section of the bar and λ_n the draw ratio in the neck. Eq. (20) can be rearranged into:

$$\frac{\sigma_{y,r}}{G_R} = \frac{\lambda_n^2 - \frac{1}{\lambda_n}}{\kappa_y \lambda_n - 1} \tag{21}$$

In Fig. 9a, Eq. (21) is represented graphically. The solid line represents the lines of equilibrium for rejuvenated ($\kappa = 1$). In the original analysis, without strain softening [39], it was already shown that for a ratio of yield stress and strain hardening modulus smaller than 3, homogenous deformation must be observed and that for a ratio above this value stable neck growth is encountered in a uniaxial tensile test. Fig. 9 shows that polycarbonate, which has a rejuvenated yield stress, $\sigma_{y,r}$ of 45 MPa and a strain hardening modulus, G_R of 29 MPa (and thus a ratio $\sigma_{y,r}/G_R$, of 1.55, indicated by the dashed line), is situated well below the equilibrium line of $\kappa = 1$. Therefore, homogeneous deformation is predicted for rejuvenated polycarbonate in uniaxial tension, which is consistent with the observations of rolled polycarbonate samples that exhibit homogeneous deformation without necking (see Fig. 8c).

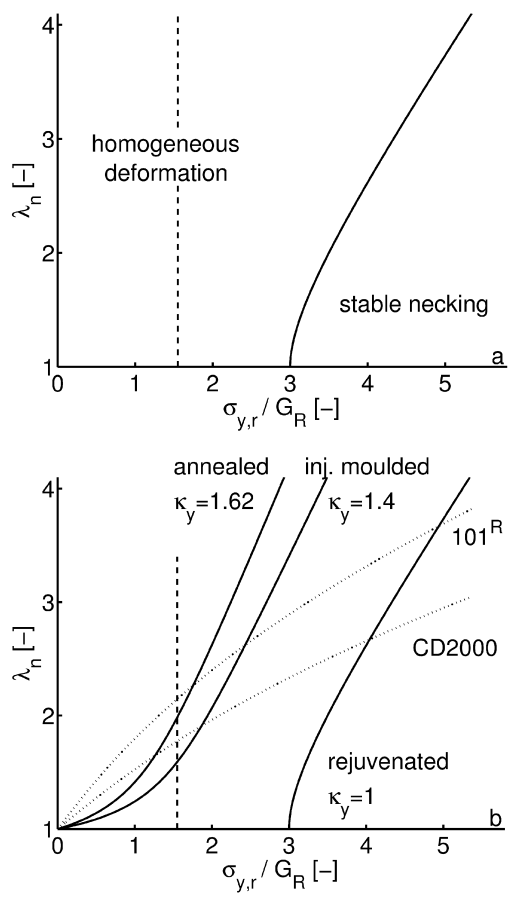

Fig. 9. Stability analysis, analogous to [38]: homogeneous deformation below a ratio $\sigma_{y,r}/G_R$ of 3 and above stable neck growth (a). Prediction of the deformation mode for two PC grades (b). Solid lines represent the equilibrium lines of stable neck growth at distinct κ_y (see Eq. (20)), the dashed line indicates a ratio $\sigma_{y,r}/G_R$ of 1.55 (characteristic for PC), and the dotted lines represent the tensile strength limits, depending on molecular weight (see Eq. (22)).

Once a polymer exhibits strain softening ($\kappa_y > 1$), the equilibrium line drops initially to zero, which, from a mechanical point of view, means that strain localisation is inevitable.

The additional solid lines in Fig. 9 represent injection-moulded polycarbonate, with a yield stress of approximately 63 MPa ($\kappa_y = 1.4$) and annealed polycarbonate, where the yield stress rises to 73 MPa ($\kappa_y = 1.62$), respectively. The dashed line and the equilibrium line intersect at a λ_n of around 1.7, approximately the draw ratio observed during neck growth (see Fig. 5). Upon annealing the equilibrium line drops further and is crossed by the dashed line at a draw ratio of 2. This illustrates that after annealing a higher load has to be transferred by the polymer network, accompanied by a higher λ_n, to stabilise the deformation.

As proposed by Flory [40] and shown for polystyrene by Merz et al. [41] and McCormick et al. [42], the tensile strength of polymers increases with the number-averaged molecular weight. The maximum stress that can be transferred by the polymer network is dependent on the molecular weight of the grade and is assumed to be equal to $\kappa_t \sigma_{y,r}$, where κ_t is a multiplier which can be determined experimentally. The tensile stress at the moment of failure equals the rejuvenated yield stress plus the stress transferred by the polymer network, which can be rearranged according to:

$$\kappa_t \sigma_{y,r} = \sigma_{y,r} + G_R\left(\lambda_n^2 - \frac{1}{\lambda_n}\right) \rightarrow \frac{\sigma_{y,r}}{G_R} = \frac{\lambda_n^2 - \frac{1}{\lambda_n}}{\kappa_t - 1} \tag{22}$$

This equation is represented by the dotted lines in Fig. 9 for Makrolon CD2000 ($\sigma_t = 120$ MPa, $\kappa_t = 2.67$) and Lexan 101^R ($\sigma_t = 165$ MPa, $\kappa_t = 3.67$) [38].

For the Lexan 101^R, with a relative high molecular weight, the tensile strength at failure is sufficiently high. However, for the Makrolon CD2000 the dotted line of tensile maximum strength is crossed by the dashed line, in case of annealing, before the equilibrium line is reached. This means that fracture occurs before the neck is stabilised (see Fig. 8b). This analysis illustrates that the embrittlement of polymers like polycarbonate in uniaxial tension, is strongly dependent in this example on the molecular weight (via κ_t) and annealing time (via κ_y).

Here it should be noted that, in contrast to the numerical model, this simple analysis does not incorporate any strain rate effects. Although these effects are small, they will lead to an overestimation of the obtained draw ratio's. It will be shown, however, that the qualitative application of such an analysis can be used effectively to rationalise the macroscopically observed tensile behaviour in terms of the measured intrinsic stress–strain properties.

3.2. Deformation and localisation processes in polystyrene

3.2.1. Results of FEM simulations

Now we investigate the influence of intrinsic properties on localisation in polystyrene (ignoring mechanisms like crazing, which will occur as a result of severe strain localisations, see for these aspects [30–32]). Fig. 10 shows the simulation of a tensile test on polystyrene. Initially the deformation is similar to polycarbonate, as shown in Fig. 4, homogeneous, elastic deformation until yielding occurs at the imperfection (see Fig. 10a). The pronounced strain softening exhibited by polystyrene, induces a much more severe localisation of strain, the stress drops drastically after yielding and hardly rises again at large strains due to insufficient strain hardening. The differences in draw ratio illustrates this the more, varying from 1 to 4 for polystyrene in Fig. 10, whereas for polycarbonate this range was only 1 to 1.8, see Fig. 4.

The deformation keeps on localising, as shown in Fig. 10b–d, without stabilisation. Ultimately, the tensile strength in the deformed region will be exceeded. At a local draw ratio of 4, close to the theoretical maximum draw ratio [1,2] the simulation is stopped. Hence, the intrinsic behaviour of polystyrene does not allow stable deformation behaviour. Its large amount of strain softening and weak strain hardening result in extreme localisation of strain which can never be stabilised. This clearly demonstrates why injection moulded polystyrene at room temperature cannot exhibit ductile or tough deformation behaviour.

3.2.2. The influence of mechanical history

Mechanical rejuvenation can also be applied to polystyrene. However, due to its craze-sensitivity this cannot be achieved by torquing and but has to be performed by rolling. This procedure, reported by Broutman for various amorphous polymers, excluding polystyrene [16,43], was applied by Govaert et al. [25] to polystyrene (N5000). They showed that a thickness reduction of 30% was sufficient to remove any strain softening in a polystyrene sample. In a subsequent tensile test, the macroscopic response of the rejuvenated material was determined where injection moulded material suffered from crazing and brittle fracture at macroscopic strain of 2% (see Fig. 11a). The rejuvenated material deformed homogeneously up to strains exceeding 30%.

As shown in Fig. 11b, pre-deformed polystyrene can be curled without the initiation of any crazing process. In Fig. 12a the stress–strain curves of polystyrene and polycarbonate tensile bars are presented, tested immediately after rolling. The yield stress has decreased dramatically and strain softening is virtually eliminated. As a consequence, homogeneous deformation is observed in these tensile tests. As mentioned before, the yield stress recovers again with ongoing time. Since the large strain behaviour remains unaffected by mechanical rejuvenation and ageing, strain softening recovers in pace with the yield stress. The yield stress as function of time after rolling (ageing time) is shown in Fig. 12b.

Although some molecular orientation occurs during rolling, this cannot be held responsible for the enhanced ductility for two reasons. Broutman et al. [16,43] demonstrated that

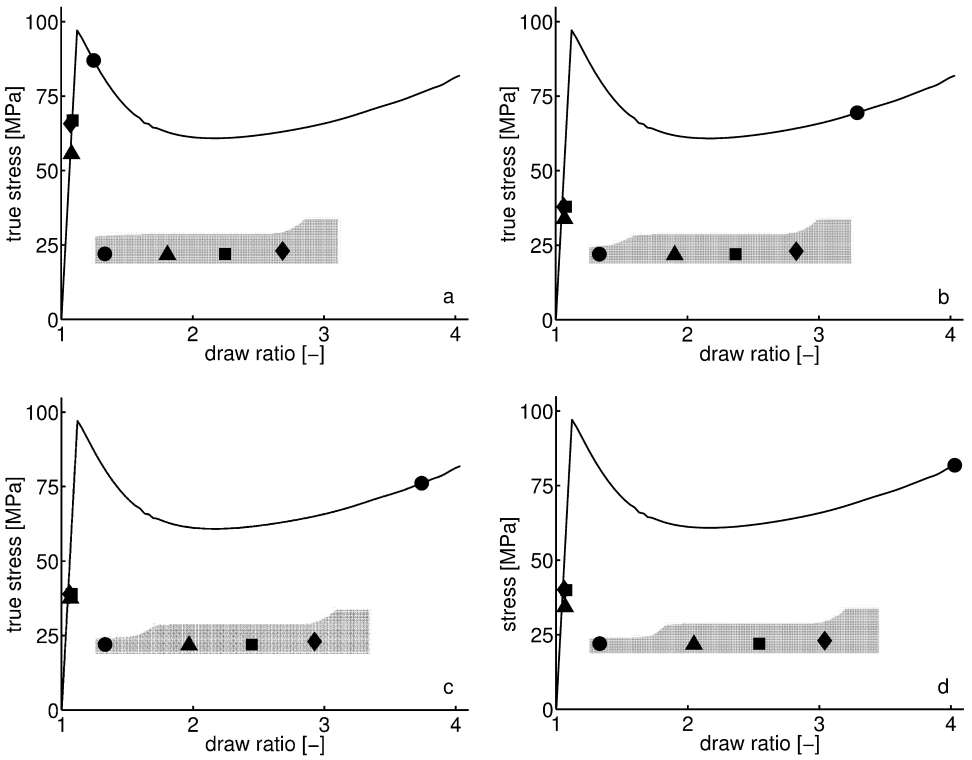

Fig. 10. Numerical simulation of a tensile test on PS: unstable growth.

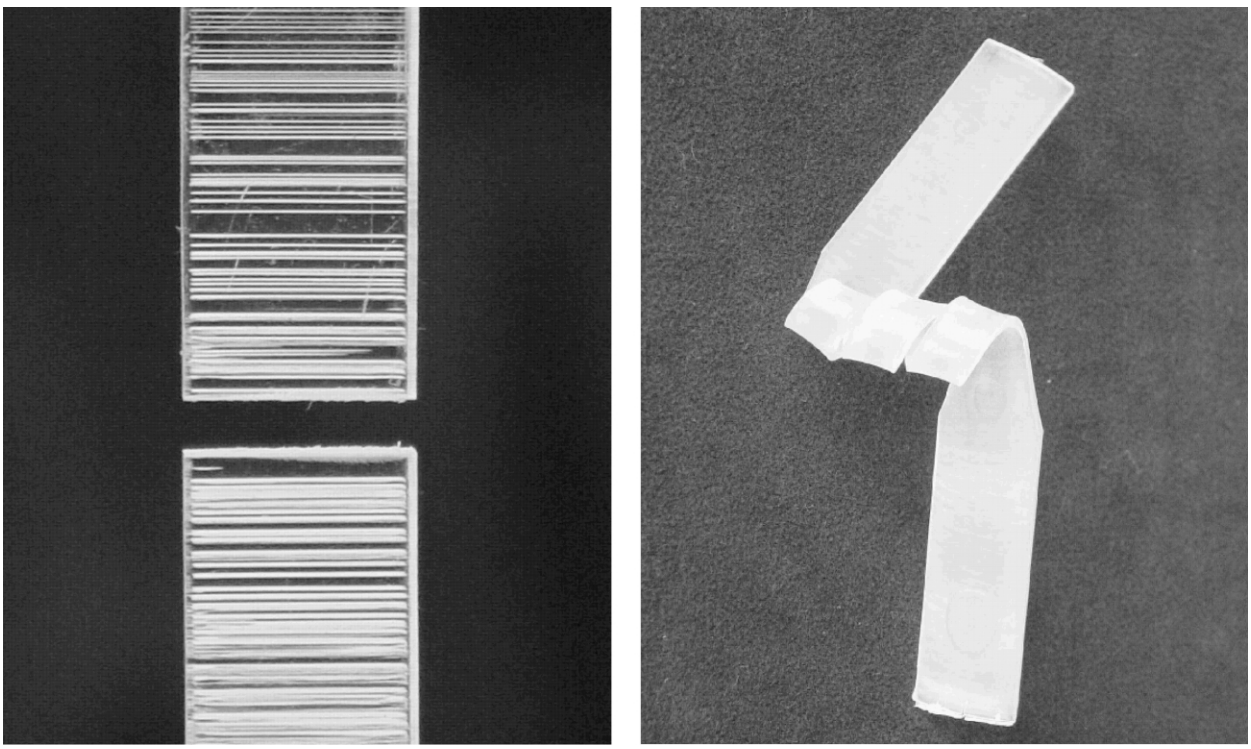

Fig. 11. Macroscopic deformation behaviour of PS, before (a) and after rolling (b).

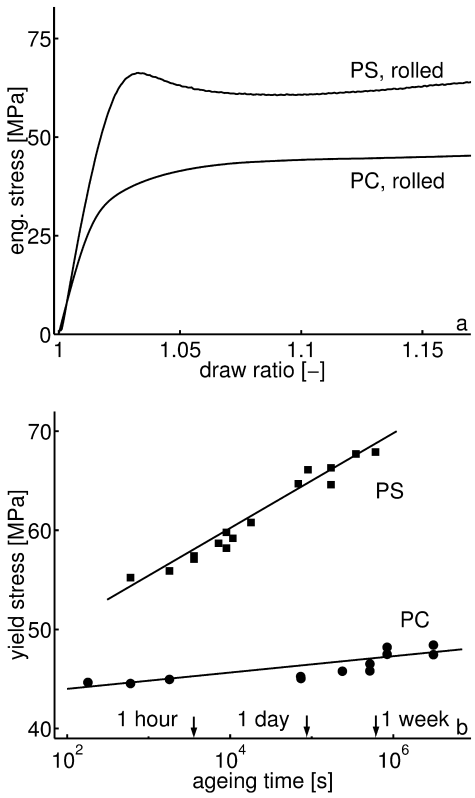

Fig. 12. Deformation behaviour (a) and ageing kinetics (b) of PS and PC after rolling. The lines in graph b are drawn as a guide to the eye.

the Izod impact strength on rolled polycarbonate is only slightly influenced by the test angle relative to the roll-direction. Moreover, the enhanced ductility and the reduction in strain softening are, similar to polycarbonate, only of temporary nature, whereas molecular orientation does not relax on this time-scale. In time, yield stress and strain softening increase, resulting in renewed localised deformation, crazing and brittle fracture on a time-scale of hours to days [44].

This graph clearly demonstrates that the recovery of yield stress in polystyrene occurs much faster than that for polycarbonate. This also explains why renewed brittle fracture returns on a much faster time-scale in polystyrene than necking in polycarbonate.

3.2.3. The influence of testing temperature

It is well known that at a temperature of 80–90 °C, a brittle-to-ductile transition is achieved in a tensile test on polystyrene [45,46]. This phenomenon originates from changes in intrinsic behaviour at this temperature, as similar to the yield stress, strain softening displays a dependence on temperature. In Fig. 2b it was already shown that for polystyrene, tested in uniaxial compression at a strain rate of 10^{-3} s^{-1}, both yield stress and strain softening decrease with increasing temperature. The amount of strain softening at 80°C is only approximately 30% of the amount of strain softening at 20 °C.

Since a reduction in strain softening can have major consequences for the macroscopic deformation behaviour, a

finite element simulation of a uniaxial tensile test on polystyrene is performed at an elevated temperature of 90 °C. Fig. 13 shows the results of this simulation. Despite the fact that the geometry of the model is identical to the geometry used in the previous simulations of Figs. 4 and 10, the slight imperfection does not induce inhomogeneous deformation at the onset of yielding (Fig. 13a) and consequently, nearly homogeneous deformation is observed during deformation, see Fig. 13b. Only the diamond marker, positioned close to the tab of the tensile bar, lays back slightly as the local cross-section reduces slower and the strain is lower in this position (Fig. 13c 13d).

This simulation is consistent with experimental observations. Tensile tests performed at temperatures ranging from 20 to 100 °C (around T_g), demonstrate that localisation of strain is indeed greatly reduced or even absent (Fig. 14a). From a testing temperature of approximately 90 °C (depending on the thermo-dynamical state of the material), similar to the numerical simulations, homogeneous deformation is observed in these tensile tests. Fig. 14b shows this temperature induced brittle-to-ductile transition for polystyrene. The exact temperature at which this transition occurs is of course also dependent of the thermo-mechanical history of the material.

3.2.4. The stabilising influence of rubber inclusions

By increasing the strain hardening contribution of the polymer network, a more stable deformation behaviour can be achieved, e.g. by cross-linking of polystyrene [7] or by blending with polyphenylene oxide (PPO) [6,9–13]. Apart

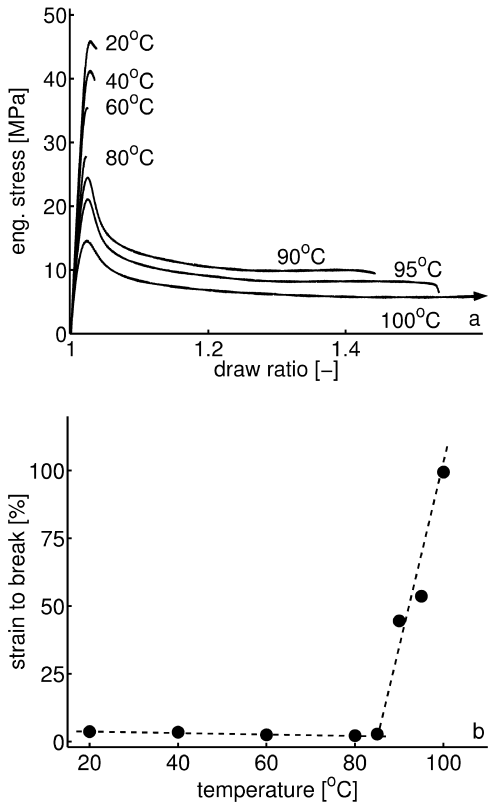

Fig. 14. Experimental tensile tests on PS at elevated temperatures (a), resulting in a brittle-to-ductile transition (b).

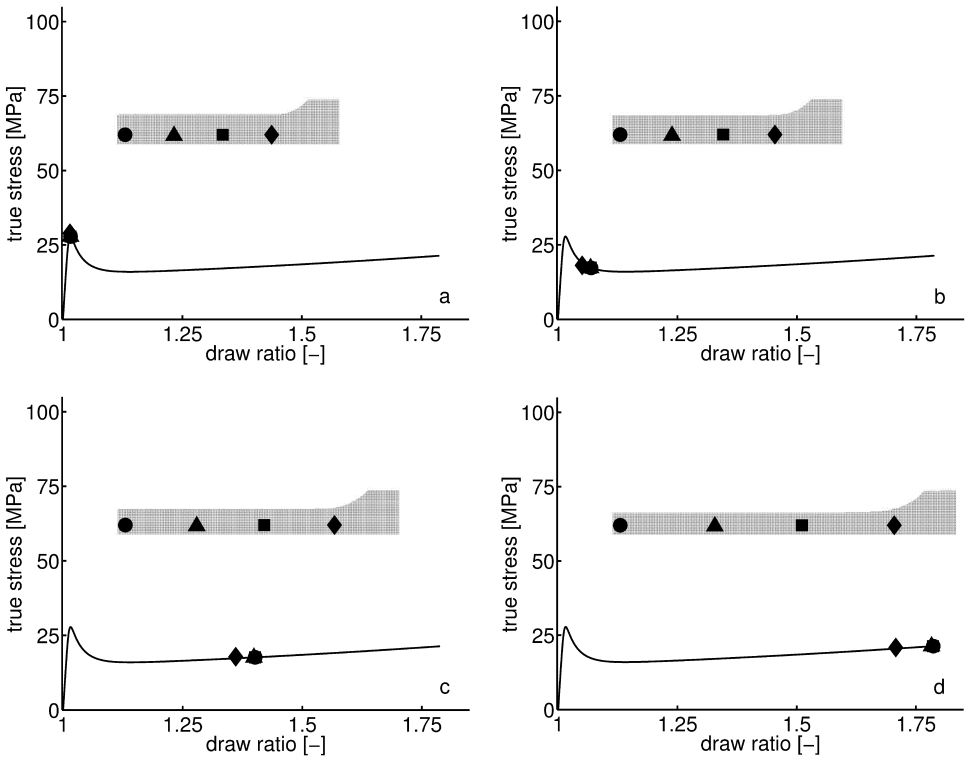

Fig. 13. Numerical simulation of a tensile test on PS at 90 °C: homogeneous deformation.

from changing the intrinsic network density of polystyrene, local strain hardening of deforming ligaments can be induced by the addition of rubber particles. Heterogeneous systems are necessary anyway to relieve local triaxial stress states in all polymer systems to circumvent defect and notch sensitivity [47–49], but this is out of the scope of the present paper. Here we only demonstrate how the ultimate impact modifier, which is a (small), core-shell rubber particle with a pre-cavitated core and a rather stiff rubbery shell [49,50] stabilises local deformation zones in polystyrene. The tensile bar now is modelled covered by a rubber layer, the thin extra layer at the surface, shown in Fig. 15. As mentioned before, this rubber shell is represented by a neo-Hookean material model, with a shear modulus of 150 MPa.

Similar to the simulations of Fig. 4, inhomogeneous deformation is induced by the imperfection at the onset of yielding (Fig. 15a). As can be seen in Fig. 15b the force transferred by the tensile bar itself is not sufficient to induce yielding in the adjacent material. However, the load bearing capacity of the rubber shell supports the deformation in the tensile bar, stabilises the neck and transfers the deformation to shoulder of the neck (Fig. 15c). Therefore, stable neck growth is observed and the entire tensile bar is plastically deformed already at a macroscopic draw ratio of approximately 2 (Fig. 15d, compare with Fig. 10b–d). A thin shell with a rather high modulus (150 MPa) was chosen here to illustrate the stabilising effect over the entire length of the tensile bar, but already for a rubber modulus of 30 MPa (of course dependent on the thickness of the layer), stabilisation is achieved. However, simulations up to very large strains would be required to visualise this stable deformation behaviour.

4. Conclusions

The macroscopic deformation behaviour of glassy polymers is dominated by the intrinsic post-yield behaviour. The subtle interplay of strain softening and strain hardening is demonstrated by finite element simulations of inhomogeneous deformation of polycarbonate in tension. Changes in strain softening due to annealing or mechanical pre-conditioning, have major consequences for the macroscopic deformation behaviour, ranging from homogeneous deformation after mechanical rejuvenation of brittle polymers to brittle fracture after annealing of ductile polymers.

A neck-stability analysis demonstrated that the macroscopic response in tension can be predicted if the intrinsic properties are known up-front. This analysis emphasises the sensitivity of the macroscopic deformation behaviour on the thermo-mechanical history and the influence of the molecular weight.

Finite element simulations of polystyrene in tension showed the extreme localisation of strain that occurs due to the pronounced strain softening and weak strain hardening. In the simulations here failure mechanism like crazing were not considered, they were a topic of a previous paper [32].

Mechanical pre-deformation of polystyrene results in

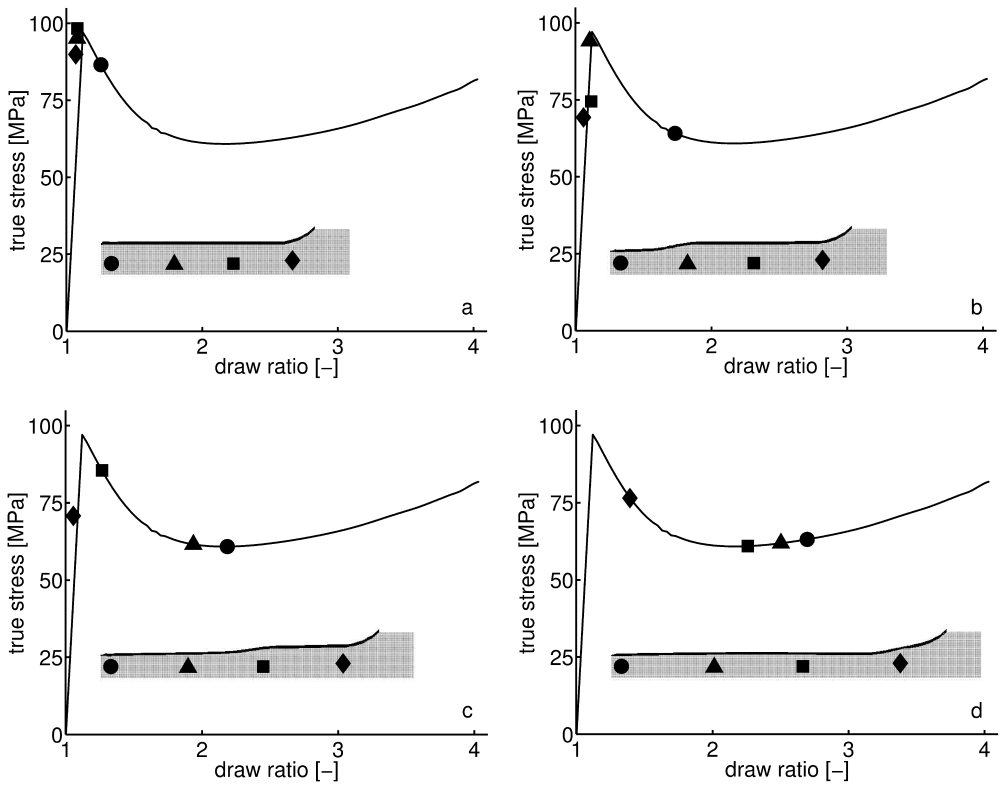

Fig. 15. Numerical simulation illustrates the stabilising effect of a rubber shell on the deformation of a PS tensile bar.

ductile deformation behaviour in tension [25]. However, this enhanced ductility is of transient nature [44]. The recovery of yield stress and strain softening results in renewed severe localisation of strain and brittle fracture. Applying a similar rolling procedure to polystyrene and polycarbonate reveals that the time-scale on which yield stress and strain softening recover are very much different. The origin of this difference in transient behaviour is most probably related to the physical origin of strain softening and a discussion on this topic can be found in [44]. Finally it is investigated how a local support of a deforming fibril by a rubber shell, part of a rubber modified material, indeed can induce delocalisation in polystyrene.

Acknowledgements

The authors wish to acknowledge the financial support provided by the Dutch Technology Foundation (STW) (Grant EWT.3766).

References

[1] Donald AM, Kramer EJ. Polymer 1982;23(3):457–60.
[2] Donald AM, Kramer EJ, Bubeck RA. J Polym Sci, Polym Phys Ed 1982;20(7):1129–41.
[3] Meijer HEH, Govaert LE, Smit RJM. A multi-level finite element method for modeling rubber-toughened amorphous polymers. In: Pearson R, editor. Toughening of plastics. Boston: American Chemical Society; 1990. p. 50–70.
[4] Haward RN, Young RJ. The physics of glassy polymers, 2nd ed. Chapman & Hall: London; 1997.
[5] Tervoort TA, Govaert LE. J Rheol 2000;44(6):1263–77.
[6] van Melick HGH, Govaert LE, Meijer HEH. Polymer 2003;44(8):2493–502.
[7] Henkee CS, Kramer EJ. J Polym Sci, Polym Phys Ed 1984;22(4):721–37.
[8] Prest jr WM, Porter RS. J Polym Sci, Part A2: Polym Phys 1972;10(9):1639–55.
[9] Donald AM, Kramer EJ. J Mater Sci 1982;17(7):1871–9.
[10] Yee AF. Polym Prepr 1976;17:145–50.
[11] Serrano AM, Welsch GE, Gibala R. Polym Engng Sci 1981;22(15):946–9.
[12] Feng H, Feng Z, Ruan H, Shen L. Macromolecules 1992;25(22):5981–5.
[13] Creton C, Halary J-L, Monnerie L. Polymer 1998;40(1):199–206.
[14] Hutchinson JM. Prog Polym Sci 1995;20(4):703–60.
[15] Struik LCE. Physical aging in amorphous polymers and other materials. Amsterdam: Elsevier; 1978.
[16] Broutman LJ, Patil RS. Polym Engng Sci 1971;11(2):165–73.
[17] Hasan OA, Boyce MC. Polymer 1993;34(24):5085–92.
[18] Xie L, Gidley DW, Hristov HA, Yee AF. J Polym Sci, Part B: Polym Phys 1995;33(1):77–84.
[19] Cross A, Haward RN, Mills NJ. Polymer 1979;20(3):288–94.
[20] Haward RN, Hay JN, Parsons IW, Adam G, Owadh AAK, Boxnyak CP, Aref-Azaf A, Cross A. Colloid Polym Sci 1980;258(6):643–62.
[21] Aboulfaraj M, G'Sell C, Mangelinck D, McKenna GB. J Non-Crystalline Solids 1994;172–174:615–21.
[22] G'Sell C. Plastic deformation of glassy polymers: constitutive equations and macromolecular mechanisms. In: McQueen H, editor. Strength of metals and alloys. Oxford: Pergamon Press; 1986. p. 1943–82.
[23] Bauwens JC. J Mater Sci 1978;13(7):1443–8.
[24] Govaert LE, Timmermans PHM, Brekelmans WAM. J Engng Mater Technol 2000;122(2):177–85.
[25] Govaert LE, van Melick HGH, Meijer HEH. Polymer 2001;42(3):1271–4.
[26] G'Sell C, Hiver JM, Dahouin A, Souahi A. J Mater Sci 1992;27(18):5031–9.
[27] Spitzig WA, Richmond O. Polym Engng Sci 1979;19:1129–39.
[28] Boyce MC, Arruda EM, Jayachandran R. Polym Engng Sci 1994;34(9):716–25.
[29] Zaroulis JS, Boyce MC. Polymer 1997;38(6):1303–15.
[30] Kramer EJ. Microscopic and molecular fundamentals of crazing. In: Kausch HH, editor. Crazing in polymers. Advances in Polymer Science, vol. 52/53. Berlin: Springer; 1983. p. 1–56.
[31] van Melick HGH, Bressers OFJT, den Toonder JMJ, Govaert LE, Meijer HEH. Polymer 2003;44(8):2481–91.
[32] van Melick HGH, Govaert LE, Meijer HEH. Polymer 2003;44(2):457–65.
[33] Tervoort TA, Smit RJM, Brekelmans WAM, Govaert LE. Mech Time-dependent Mater 1998;1(3):269–91.
[34] Eyring H. J Chem Phys 1936;4:283–91.
[35] Hasan OA, Boyce MC, Li XS, Berko S. J Polym Sci, Part B: Polym Phys 1993;31(2):185–97.
[36] van Krevelen DW. Properties of polymers. Amsterdam: Elsevier; 1972.
[37] Klompen ETJ. Deformation behaviour of glassy polymers: consequences of thermorheological complex behaviour. Institute for Continuing Education, Eindhoven University of Technology; 1996.
[38] Govaert LE, van Aert CAC, Boekholt J. Proceedings of the 10th International Conference on Deformation, Yield and Fracture of Polymers. Cambridge, United Kingdom: The Institute of Materials; 1997. p. 423–6.
[39] Haward RN. Polymer 1987;28:1485–8.
[40] Flory PJ. J Am Chem Soc 1945;67:2048–50.
[41] Merz EH, Nielsen LE, Buchdahl R. Ind Engng Chem 1951;43:1396–401.
[42] McCormick HW, Brower FM, Kin L. J Polym Sci 1959;39:87–100.
[43] Broutman LJ, Krishnakumar SM. Polym Engng Sci 1974;14(4):249–59.
[44] van Melick HGH, Raas B, Nauta WJ, Govaert LE, Meijer HEH. Polymer 2003;44(4):1171–9.
[45] Vincent PI. Polymer 1960;1:425–44.
[46] Matsushige K, Radcliffe SV, Baer E. J Appl Polym Sci 1976;20:1853–66.
[47] Smit RJM, Brekelmans WAM, Meijer HEH. J Mater Sci 2000;35(11):2855–67.
[48] Smit RJM, Brekelmans WAM, Meijer HEH. J Mater Sci 2000;35(11):2869–79.
[49] Smit RJM, Brekelmans WAM, Meijer HEH. J Mater Sci 2000;35(11):2881–92.
[50] Jansen BJP, Rastogi S, Meijer HEH, Lemstra PJ. Macromolecules 2001;34:3998–4006.